

# Surface structure in simple liquid metals. An orbital free first principles study.

D.J. González<sup>1</sup> L.E. González<sup>1</sup>, and M.J. Stott<sup>2</sup>

<sup>1</sup>*Departamento de Física Teórica, Facultad de Ciencias,  
Universidad de Valladolid, 47011 VA, SPAIN. and*

<sup>2</sup>*Department of Physics, Queen's University, Kingston, Ontario K7L 3N6 CANADA*

(Dated: June 8, 2018)

Molecular dynamics simulations of the liquid-vapour interfaces in simple *sp*-bonded liquid metals have been performed using first principles methods. Results are presented for liquid Li, Na, K, Rb, Cs, Mg, Ba, Al, Tl, and Si at thermodynamic conditions near their respective triple points, for samples of 2000 particles in a slab geometry. The longitudinal ionic density profiles exhibit a pronounced stratification extending several atomic diameters into the bulk, which is a feature already experimentally observed in liquid K, Ga, In, Sn and Hg. The wavelength of the ionic oscillations shows a good scaling with the radii of the associated Wigner-Seitz spheres. The structural rearrangements at the interface are analyzed in terms of the transverse pair correlation function, the coordination number and the bond-angle distribution between nearest neighbors. The valence electronic density profile also shows (weaker) oscillations whose phase, with respect to those of the ionic profile, changes from opposite phase in the alkalis to almost in-phase for Si.

PACS numbers: 61.25.Mv, 64.70.Fx, 71.15.Pd

## I. INTRODUCTION

The study of the structure of the free liquid surface has attracted much theoretical and experimental work,<sup>1,2</sup> with emphasis on the possible existence of liquid surface layers. Although it is by now well established that ionic<sup>3</sup> and dielectric<sup>1,4</sup> liquids exhibit just a smooth monotonic decay from the bulk liquid density to the bulk vapour density, liquid surface layering appears in liquid crystals<sup>5</sup> and at the interface between a simple fluid and a hard wall<sup>6</sup>. Understandably, special attention has been devoted to liquid metals since the early experiments suggested a liquid surface layered structure in Hg<sup>7</sup>; computer simulation<sup>8,9,10,11,12,13</sup> and theoretical studies<sup>14</sup> predicted a significant structure, extending several atomic layers into the bulk liquid. These results have been recently corroborated by X-ray reflectivity experiments on liquid Hg, Ga, In, Sn, K and Na<sub>0.33</sub> K<sub>0.67</sub>.<sup>15</sup>

It not yet settled whether surface layering is a feature of all liquid metals or only characteristic of some. Rice and coworkers<sup>8,9,10</sup> have performed Monte Carlo (MC) simulations based on density-dependent pair potentials obtained from pseudopotentials; their results suggest that surface layering is due to the coupling between ionic and electronic density profiles (DP) and that the abrupt decay of the electron DP gives rise to an effective wall against which the ions, behaving like hard-spheres, stack. Other workers<sup>16</sup> have suggested that the many body forces arising from the delocalized electrons, tend to increase the ionic surface density so that its coordination approaches that of the bulk. Recently, Chacon *et al*<sup>17</sup> proposed that surface layering may be a generic property of fluids at low temperature, so that the only requirement for an oscillatory DP is a low melting temperature relative to the critical temperature so as to avoid crystallization.

This paper reports a study on the liquid-vapour in-

terface of several simple *sp*-bonded liquid metals at thermodynamic conditions near their respective triple points. The study has been carried out by using the orbital-free *ab initio* molecular dynamics (OF-AIMD) method, where the forces acting on the nuclei are computed from electronic structure calculations, based on density functional theory (DFT)<sup>18</sup>, which are performed as the MD trajectory is generated. Large samples and long MD simulation times are possible when interatomic pair potentials are used to describe the effective ion-ion interactions; however at a liquid metal surface this approximation becomes unreliable as the electron density sharply drops from its bulk value to zero outside the surface. In these circumstances it is vital to allow the forces on the atoms to respond to the electron density distribution in their vicinity. At present the best way of accomplishing this goal is by resorting to first-principles molecular dynamics techniques, where the electronic density, total energy and forces are obtained by using the Kohn-Sham (KS) formulation of the density functional theory (DFT).<sup>18</sup> However, the computational demands of these *ab-initio* methods, where KS orbitals are used to describe the electronic density and to compute exactly the electronic kinetic energy, grow very rapidly with system size, and their memory requirement is also quite large. These considerations have posed important constraints on both the sizes of the systems studied so far, as well as the simulation times. Heretofore, only two KS-AIMD calculations have been performed on the liquid-vapour (LV) interfaces of liquid metals. Fabricius *et al*<sup>11</sup> have studied the LV interface in liquid silicon near melting by using 96 particles and a total simulation time of 30 ps. Likewise, Walker *et al*<sup>12</sup> have studied the LV surface in liquid sodium near melting by a simulation which used 160 particles and lasted 50 ps. In both studies, the size limitations materialized in small simulation slabs ( $\approx 12.0$  Å thick for Si and 22.0 Å thick for Na) which may rise some reasonable ques-

tions about its capability to simulate a real macroscopic LV interface, as the small thickness makes plausible the existence of interactions between both sides of the slab.

However, the aforementioned limitations can be partly overcome if the exact calculation of the electronic kinetic energy is given up in favor of an approximate kinetic energy functional of the electronic density. This is the philosophy behind the so-called orbital-free *ab initio* molecular dynamics (OF-AIMD) method<sup>19,20</sup>, which by eliminating the orbitals of the KS formulation provides a simulation method where the number of variables describing the electronic state is greatly reduced, enabling the study of larger samples and for longer simulation times. Although the OF-AIMD method uses an explicit approximation for the electronic kinetic energy functional of DFT, nonetheless it correctly treats the forces on the ions. We stress that, although less demanding than KS-AIMD, the OF-AIMD method is still much more costly than the use of pair potentials; however, recent calculations have succeeded to use 2000 and 3000 particles to study the surface properties of several simple liquid metals and binary alloys,<sup>13</sup> namely, Li, Na, Mg, Al, Si, Na<sub>0.3</sub>K<sub>0.7</sub> and Li<sub>0.4</sub>Na<sub>0.6</sub>.

The OF-AIMD results for Na and Si, when compared with experimental data (as the surface tension) and with the in principle more accurate KS-AIMD results (as the density profiles) for the same systems, can be used as a validation test of the method, as far as the study of metallic surface properties is concerned. As we show below in detail, several magnitudes are very similar: the oscillating profiles, and in particular the wavelength of the oscillations, which is recovered exactly, the number of neighbors of a Si atom across the interface, and the surface tension of liquid Na, are all well reproduced by the OF-AIMD approach. Further confidence in the capabilities of the OF-AIMD method in relation to surface properties is obtained from results for metallic clusters (finite systems where the surface is indeed utmost important). For instance, a long standing, previously unexplained, anomalous variation of the melting temperature of Na clusters with size<sup>21</sup> has been for the first time reproduced and rationalized in terms of surface geometry and stability<sup>22</sup> using the OF-AIMD method with the same kinetic energy functional used in the present work.

We do consider that reproduction of the surface properties of finite systems is much more stringent a test than the reproduction of the surface properties of a semiinfinite solid surface. Nevertheless, in order to satisfy the requirements of one referee and to further reassess for the readers the capabilities of the OFAIMD method, we have performed preliminary studies of the properties of some open metallic solid surfaces, as the (110) surface of fcc Al and the (10 $\bar{1}$ 0) surface of hcp Mg.<sup>23</sup> In both cases, experimental measurements<sup>24,25</sup> show that surface relaxation leads to a contraction of the first interlayer distance, expansion of the second interlayer distance, contraction of the third, and so on. Moreover, the thermal expansion coefficient in the case of Al (110) is negative,

positive and positive for the first, second and third interdistances, while for Mg (10 $\bar{1}$ 0) an oscillatory behavior is found starting with a negative thermal expansion coefficient. KS-AIMD simulations for several temperatures were performed<sup>26</sup> for Al (110) using 8 layers with 9 atoms in each one plus a vacuum of 8.5 Å, reproducing the experimental trends. Our OF-AIMD calculations, using the same simulation setup, also reproduce both the sign of the relaxations and their thermal behaviour. Theoretical calculations within the quasiharmonic approximation, based on KS *ab initio* static calculations (not MD simulations),<sup>25</sup> were also able to reproduce the experimental behavior of Mg (10 $\bar{1}$ 0). Our OF-AIMD data again reproduce qualitatively the experimental trends, with both oscillatory relaxations and thermal expansion coefficients. Further details and analysis of the data will be presented elsewhere.

In our previous OF-AIMD studies of liquid metallic surfaces<sup>13</sup> we first of all proved the feasibility of performing *ab initio* simulations for large systems, including one component metals and alloys, we showed that different ordering properties in the case of alloys lead to substantial differences in the partial and total density profiles, and studied the evolution of the relationship between ionic and valence electron density profiles as the valence of the metal is increased in the series Li, Mg, Al, Si. Here we extend the number of systems studied, we analyze in detail the structure of the systems, both perpendicular and parallel to the interface, and complete the study of the electronic density profiles, stressing the evolution of these properties as the atomic valence is varied.

## II. THEORY

A simple liquid metal is treated as a disordered array of  $N$  bare ions with valence  $Z$ , enclosed in a volume  $V$ , and interacting with  $N_e = NZ$  valence electrons through an electron-ion potential  $v(r)$ . The total potential energy of the system can be written, within the Born-Oppenheimer approximation, as the sum of the direct ion-ion coulombic interaction energy and the ground state energy of the electronic system under the external potential created by the ions,  $V_{\text{ext}}(\vec{r}, \{\vec{R}_l\}) = \sum_{i=1}^N v(|\vec{r} - \vec{R}_i|)$ ,

$$E(\{\vec{R}_l\}) = \sum_{i < j} \frac{Z^2}{|\vec{R}_i - \vec{R}_j|} + E_g[\rho_g(\vec{r}), V_{\text{ext}}(\vec{r}, \{\vec{R}_l\})], \quad (1)$$

where  $\rho_g(\vec{r})$  is the ground state electronic density and  $\vec{R}_l$  are the ionic positions.

According to DFT, the ground state electronic density,  $\rho_g(\vec{r})$ , can be obtained by minimizing the energy functional  $E[\rho]$ , which can be written

$$E[\rho(\vec{r})] = T_s[\rho] + E_H[\rho] + E_{\text{xc}}[\rho] + E_{\text{ext}}[\rho] \quad (2)$$

where the terms represent, respectively, the electronic kinetic energy,  $T_s[\rho]$ , of a non-interacting system of density  $\rho(\vec{r})$ , the classical electrostatic energy (Hartree term),

$$E_H[\rho] = \frac{1}{2} \int \int d\vec{r} d\vec{s} \frac{\rho(\vec{r})\rho(\vec{s})}{|\vec{r} - \vec{s}|}, \quad (3)$$

the exchange-correlation energy,  $E_{xc}[\rho]$ , for which we have adopted the local density approximation and finally the electron-ion interaction energy,  $E_{\text{ext}}[\rho]$ , where the electron-ion potential has been characterized by a local ionic pseudopotential which has been constructed within DFT<sup>19</sup>.

$$E_{\text{ext}}[\rho] = \int d\vec{r} \rho(\vec{r}) V_{\text{ext}}(\vec{r}), \quad (4)$$

In the KS-DFT method,<sup>18</sup>  $T_s[\rho]$  is calculated exactly by using single particle orbitals, which requires huge computational effort. This is alleviated in the OF-AIMD approach<sup>18,19,20</sup> by use of an explicit but approximate functional of the density for  $T_s[\rho]$ . Proposed functionals consist of the von Weizsäcker term,

$$T_W[\rho(\vec{r})] = \frac{1}{8} \int d\vec{r} |\nabla \rho(\vec{r})|^2 / \rho(\vec{r}), \quad (5)$$

plus further terms chosen in order to reproduce correctly some exactly known limits. Here, we have used an average density model<sup>19</sup>, where  $T_s = T_W + T_\beta$ ,

$$T_\beta = \frac{3}{10} \int d\vec{r} \rho(\vec{r})^{5/3-2\beta} \tilde{k}(\vec{r})^2 \quad (6)$$

$$\tilde{k}(\vec{r}) = (2k_F^0)^3 \int d\vec{s} k(\vec{s}) w_\beta(2k_F^0|\vec{r} - \vec{s}|)$$

$k(\vec{r}) = (3\pi^2)^{1/3} \rho(\vec{r})^\beta$ ,  $k_F^0$  is the Fermi wavevector for mean electron density  $\rho_e = N_e/V$ , and  $w_\beta(x)$  is a weight function chosen so that both the linear response theory and Thomas-Fermi limits are correctly recovered. Further details are given in reference [19].

Another key ingredient of the energy functional is the local ion pseudopotential,  $v_{ps}(r)$ , describing the ion-electron interaction. For each system, the  $v_{ps}(r)$  has been constructed from first principles by fitting, within the same  $T_s[\rho]$  functional, the displaced valence electronic density induced by an ion embedded in a metallic medium as obtained in a KS calculation which, moreover, also gives the corresponding core electronic density. Further details on the construction of the pseudopotential are given in reference [19] and we just note that the previous theoretical framework has already provided an accurate description of several static and dynamic properties of bulk liquid Li, Mg, Al, Si, Na-Cs and Li-Na systems<sup>19,27,28</sup>.

TABLE I: Input data for the simple metals studied in this work, along with some simulation details.  $\delta t$  is the ionic time step in ps, the cutoff energy,  $E_{\text{Cut}}$ , is given in Ryd, and  $N_{\text{Conf}}$  is the total number of configurations.

Metal	$\rho$ ( $\text{\AA}^{-3}$ )	T (K)	$L_0$ ( $\text{\AA}$ )	$\alpha$	$\delta t$	$E_{\text{Cut}}$	$N_{\text{Conf}}$
Li	0.0445	470	28.44	1.95	0.0060	9.50	18000
Na	0.0242	373	33.50	2.20	0.0025	7.50	24700
K	0.0127	343	44.99	1.73	0.0050	5.25	25100
Rb	0.0103	315	48.26	1.73	0.0065	5.25	22100
Cs	0.0083	303	51.77	1.73	0.0050	4.74	18300
Mg	0.0383	953	29.90	1.95	0.0010	8.50	22000
Ba	0.0146	1003	43.00	1.73	0.0040	4.95	21000
Al	0.0529	943	28.97	1.56	0.0010	11.25	20000
Tl	0.0332	590	32.53	1.75	0.0075	10.50	30000
Si	0.0555	1740	27.41	1.75	0.0035	15.55	20000

### III. RESULTS

We have performed OF-AIMD simulations for the LV interfaces in the liquid metals Li, Na, K, Rb, Cs, Mg, Ba, Al, Tl and Si at thermodynamic conditions near their experimental triple points. For each system we have considered a slab consisting of 2000 ions in a supercell with two free surfaces normal to the  $z$ -axis. The dimensions of the slab were  $L_0 \cdot L_0 \cdot L_z$  ( $L_z = \alpha L_0$ ), with  $L_0$  and  $\alpha$  chosen so that the average number density of the slab coincides with the experimental bulk ionic number density of the system at the same temperature; additional details about the thermodynamic states are given in Table I along with several simulation parameters. A further 8  $\text{\AA}$  of vacuum were added both above and below the slab. Therefore, we are dealing with liquid slabs which are wide enough to rule out interference effects between the two free surfaces and with supercells which are large enough to discard slab-slab interactions. Although the periodic boundary conditions require that a particle moving out of the cell in the  $z$ -direction reappears on the other side of the slab, we did not observe such event during the present simulations. Given the ionic positions at time  $t$ , the electron density was expanded in plane waves and the energy functional was minimized with respect to the plane wave coefficients yielding the ground state electronic density, energy, and the forces on the ions, and therefrom the ionic positions and velocities were updated according to Newton equations, i.e., the simulations are performed in the NVE ensemble. For all systems equilibration runs were previously performed for a range between 2000-4000 configurations, depending on the system. Therefrom, the  $N_{\text{Conf}}$  ensuing configurations were those used in the evaluation of the slab's physical properties.

During the simulations each slab contracted or expanded and the average ionic density varied in response to the condition of zero external pressure so that the ionic density in the central region of slab changed by an amount ranging from  $\approx -1.5\%$  in Tl to  $\approx 20\%$  in K and

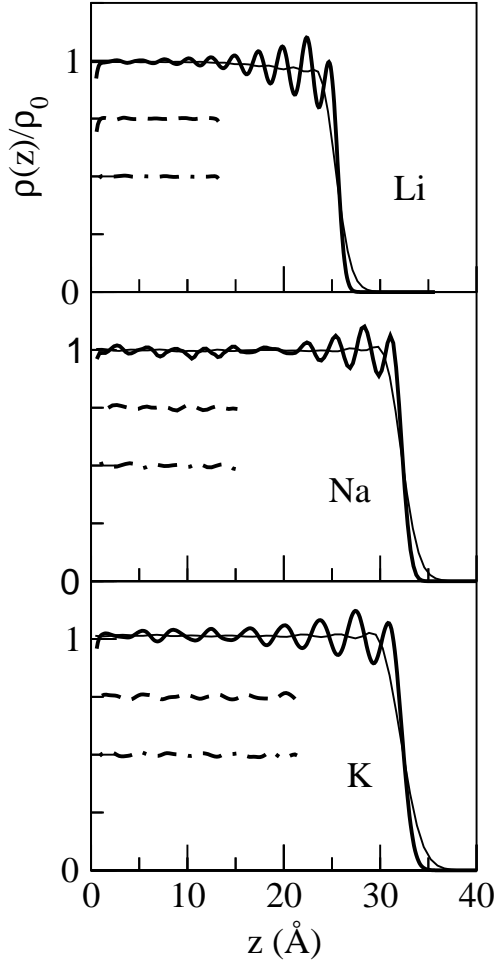


FIG. 1: Electronic (dotted line) and ionic (full line) density profiles normal to the liquid-vapour interface in the Li, Na and K liquid metals. The densities are plotted relative to their respective bulk values. The dashed and dot-dashed lines are the  $x$ -transverse (displaced by  $-0.25$ ) and  $y$ -transverse (displaced by  $-0.5$ ) ionic density profiles.

Si.

#### A. Ionic density profiles.

The longitudinal ionic DP were computed from a histogram of particle positions relative to the slab's center of mass, with the profiles from both halves of the slab being averaged, and the obtained results are shown in figures 1- 5. All systems show a stratification for at least four layers into the bulk liquid, a structural feature that has already been observed experimentally for the LV interface of Hg, Ga, In, Sn, K and  $\text{Na}_{33}\text{K}_{67}$ <sup>15</sup>.

The wavelength,  $\lambda$ , of the ionic oscillations is given in Table II, and its values scale linearly with the radii of the Wigner-Seitz spheres,  $R_{\text{WS}}$ , while it shows no definite relationship with electronic parameters, like the radii per

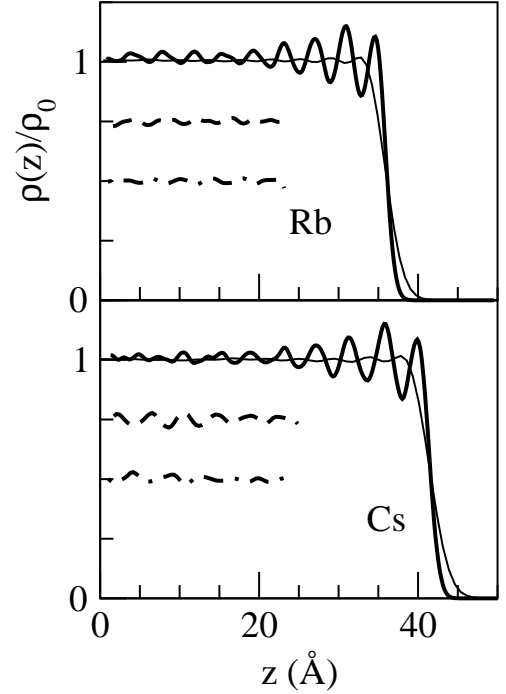


FIG. 2: Same as the previous figure but for the Rb and Cs liquid-vapour interfaces.

electron,  $r_s$  (see figure 6). This result suggests that the ionic oscillations are not a consequence of Friedel oscillations in the electronic density, but on the contrary they are due to atomic stacking against the surface. Parenthetically, we mention that the present OF-AIMD values of  $\lambda$  for Na (3.0 Å) and Si (2.5 Å) exactly coincide with the values derived in KS-AIMD type calculations.<sup>11,12</sup>

Another noticeable feature of the ionic DPs refers to the relative amplitudes of the first and second oscillations near the LV interface. Within the group of the alkali metals, we observe that the amplitude of the first oscillation is smaller than that of the second oscillation; this feature is more marked in Li and is much smaller for the other alkalis. Conversely, for Mg we obtain a first oscillation whose amplitude is slightly larger than that of the second albeit this effect is reversed in Ba. However, for Al, Tl and Si we obtain a first oscillation with an amplitude clearly larger than that of the second oscillation. Indeed, the present results suggest that as the valence of the system increases so does the ratio between the amplitudes of the first and second oscillations in the longitudinal ionic DP.

The OF-AIMD results for the alkalis closely agree with previous MC results of Rice *et al*<sup>8,9,10</sup> for Na, K, Rb and Cs, where the first oscillation had a shorter amplitude than the second. Furthermore, their MC results for Al, Ga, In and Tl<sup>10</sup> showed a first oscillation with a larger amplitude than the second, which again coincides with the OF-AIMD results for Al and Tl, and most importantly, this trend is also visible in the reported ex-

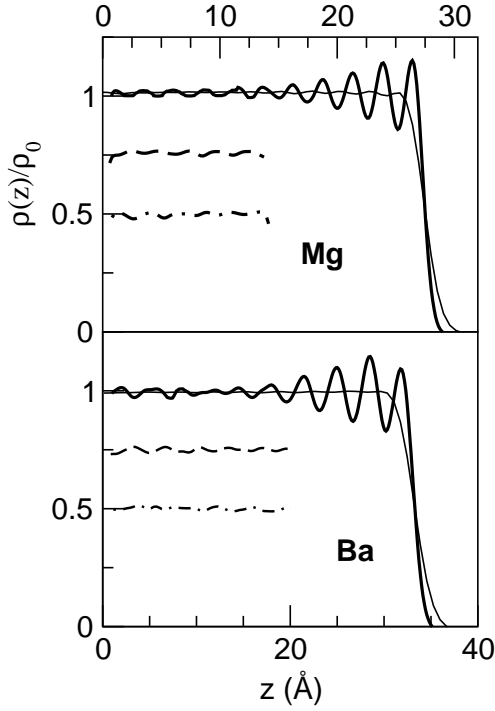


FIG. 3: Same as the previous figure but for the Mg and Ba liquid-vapour interfaces. Notice the different  $x$ -axis scales.

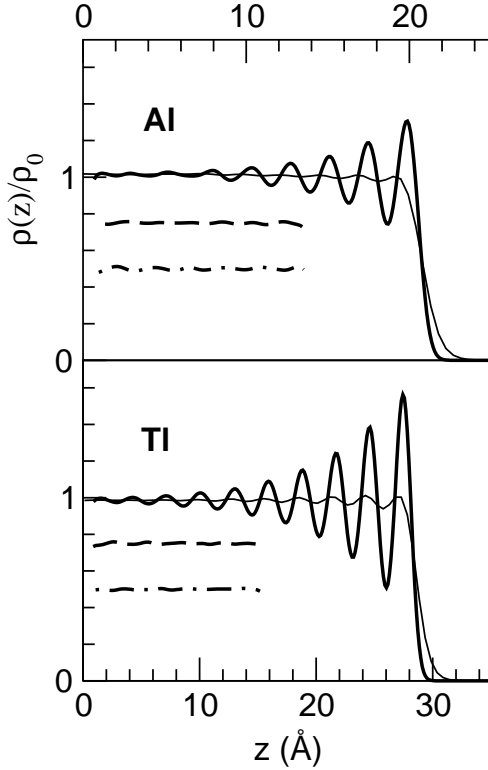


FIG. 4: Same as the previous figure but for the Al and Tl liquid-vapour interfaces. Notice the different  $x$ -axis scales.

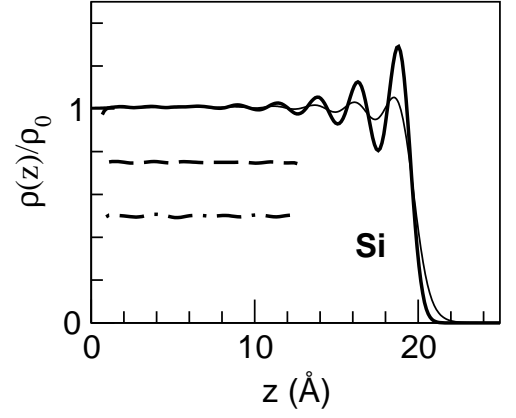


FIG. 5: Same as the previous figure but for the Si liquid-vapour interfaces.

TABLE II: Information about several properties of the slabs.  $\rho$  is the ionic number density in a wide central region of the slab,  $\Delta\rho$  is its variation with respect to the input ionic density,  $\lambda$  is the wavelength of the longitudinal ionic oscillations, and  $\sigma$  denotes the pseudoatom size (see text).

Metal	$\rho$ ( $\text{\AA}^{-3}$ )	$\Delta\rho$ (%)	$\lambda$ ( $\text{\AA}$ )	$\sigma$ ( $\text{\AA}$ )	$\sigma/\lambda$
Li	0.0478	7.6	2.5	1.601	0.640
Na	0.0272	12.0	3.0	1.859	0.620
K	0.0152	19.4	3.7	2.309	0.624
Rb	0.0118	14.4	3.9	2.458	0.630
Cs	0.0089	7.2	4.3	2.710	0.630
Mg	0.0404	5.5	2.6	1.500	0.577
Ba	0.0162	11.1	3.6	2.120	0.589
Al	0.0570	7.2	2.35	1.288	0.548
Tl	0.0328	-1.5	2.90	1.274	0.440
Si	0.0666	20.0	2.5	1.132	0.453

perimental longitudinal ionic DP for Hg, Ga and In<sup>15</sup>. Likewise, we note that both the present OF-AIMD and the MC results, have yielded a first oscillation which is more marked in Tl than Al. On the other hand, the recent KS-AIMD simulation<sup>12</sup> for the LV interface in Na, has also produced an oscillatory longitudinal ionic DP with a first oscillation having an amplitude slightly larger than that of the second.

Besides the correlation found between the amplitudes of the first and second oscillations and the valence of the system, we have also unveiled another correlation concerning the decaying tail of the ionic DPs in the LV interface region. Specifically, when the ionic DPs are scaled in terms of their respective wavelength,  $\lambda$ , it is found that the decaying tail of  $\rho(z/\lambda)$  is virtually the same for all the systems with the same valence,  $Z$ , and moreover this tail becomes steeper with increasing  $Z$ .

We have also checked that the stratification of the ionic DPs is not an artifact induced by the finite size of the simulation box. Therefore, we have computed the trans-

TABLE III: Details of the layers used for computing the transverse pair correlation functions.  $\Delta z_{OL}$  and  $\Delta z_{SL}$  refer to the positions, with respect to the center of mass, of the outermost and second layers, respectively.  $\Delta \rho_{OL}$  and  $\Delta \rho_{SL}$  are the percent variations, with respect to the slab's bulk value, of the ionic number densities in the outermost and second layers, respectively.

Metal	$\Delta z_{OL}$ (Å)	$\Delta z_{SL}$ (Å)	$\Delta \rho_{OL}$	$\Delta \rho_{SL}$
Li	23.6-25.7	21.1-23.6	-11.3	-2.3
Na	29.9-32.4	26.9-29.9	-6.9	0.0
K	29.3-32.4	25.6-29.3	-8.1	-0.5
Rb	32.8-36.1	28.9-32.8	-7.2	0.0
Cs	37.9-41.7	33.6-37.9	-9.4	0.0
Mg	25.2-27.6	22.6-25.2	-6.5	-1.0
Ba	30.2-33.4	26.6-30.2	-7.7	-0.6
Al	18.7-20.8	16.35-18.7	+4.0	-1.0
Tl	26.0-28.5	23.1-26.0	+9.0	-1.2
Si	17.5-19.8	15.0-17.5	+0.6	-1.5

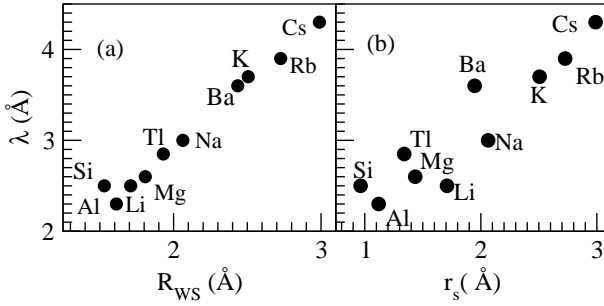


FIG. 6: Wavelength of the longitudinal ionic oscillations as a function of (a) the radius of the respective Wigner-Seitz spheres,  $R_{WS}$  (b) the radius of a sphere which on average contains one electron,  $r_s$ .

verse ionic DPs which, as shown in figures 1-5, are more or less uniform, albeit with some noise which is always substantially smaller than the amplitudes of the oscillations in the corresponding longitudinal DP. As a further check on the reliability of the present calculations, we have also calculated the corresponding *bulk* pair distribution functions,  $g(r)$ , which have been evaluated within a 30.0 Å wide central section of the corresponding slab. The obtained results are depicted in figures 7- 9 along with their experimental counterparts<sup>30</sup>. The small mismatch observed in Mg, Ba and Al may be ascribed to the aforementioned increase in the average ionic density in the central part of the slab.

### B. Atomic structure of the layers.

The planar LV interfaces considered in this work are inhomogeneous systems along the  $z$  direction, but isotropic and homogeneous on the  $xy$  planes; consequently the

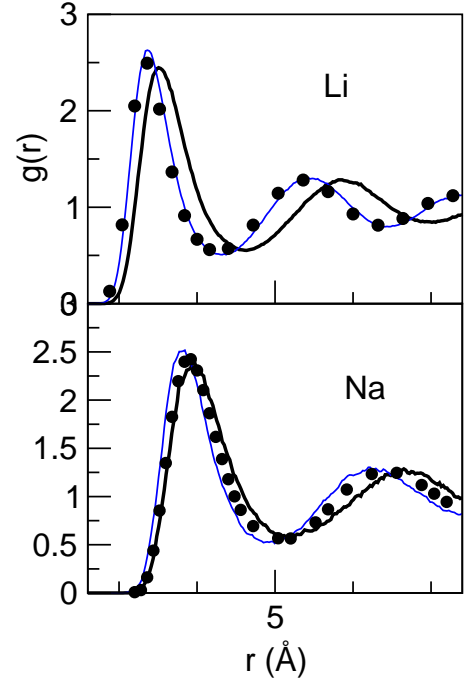


FIG. 7: (Color online) Transverse pair correlation functions for selected layers of the Li and Na slabs, namely from the bulk (thin blue line) and from the outermost layer (thick line). The full circles stand for the bulk experimental data.

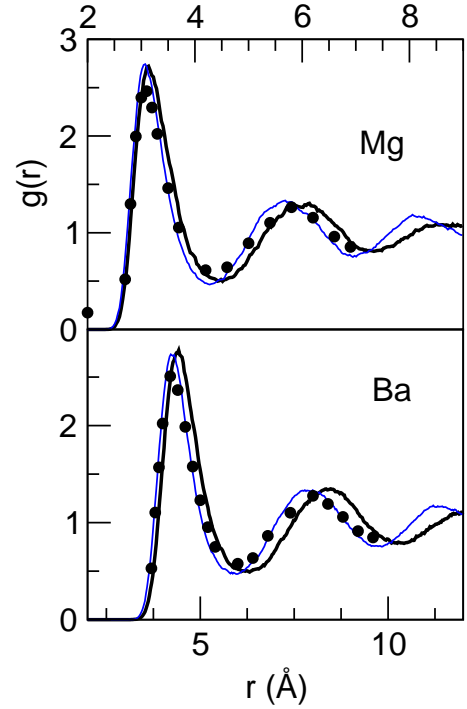


FIG. 8: (Color online) Same as the previous figure but for liquid Mg and Ba.

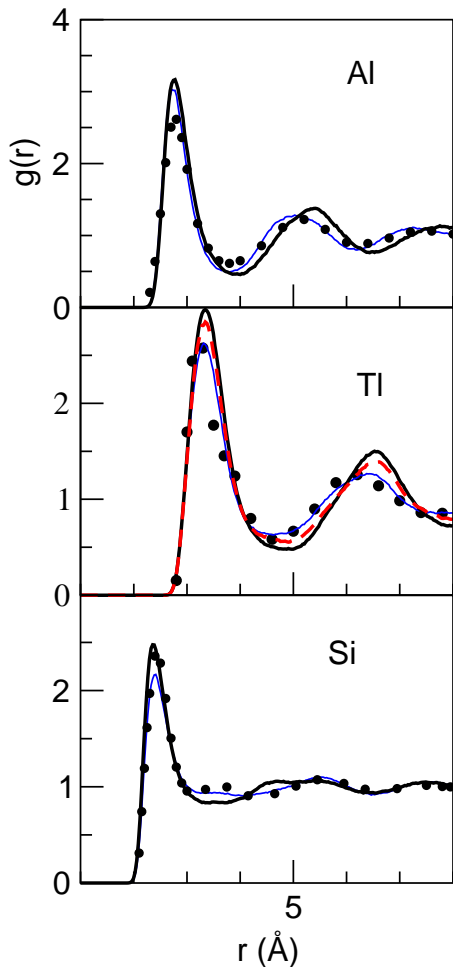


FIG. 9: (Color online) Same as the previous figure but for liquid Al, Tl and Si. In Tl the dashed red line is the  $g_T(r)$  of the second layer.

two-body distribution functions, which provide information about the atomic structure, depend on the  $z$  coordinates of the two particles and on the transverse distance between them, i.e.  $g(\vec{r}_1, \vec{r}_2) = g(z_1, z_2, R_{12})$  where  $R_{12} = \sqrt{(x_2 - x_1)^2 + (y_2 - y_1)^2}$ . The three body distribution functions, as for instance the bond-angle distribution, also display similar symmetry properties.

However, such a detailed description of the structure is difficult to obtain from the simulations, so below we consider several averaged magnitudes in which the average is taken over a given layer or slice of the simulation slab. The first (or outermost) layer comprises the region from the outermost minimum of the ionic DP to its inflection point in the decaying tail. The other layers are located between consecutive minima of the ionic oscillations. For a given metal, all the layers have the same width (excepting the outermost one which is always slightly narrower) and its specific values are given in Table III. Furthermore, in order to achieve meaningful comparisons we have also considered a layer with the

same width and located in the central bulk region, which will be termed the “center layer”.

A first magnitude to analyze is the average ionic density within each layer. Another one is the transverse pair correlation function  $g_T(r)$ , which accounts for the probability of finding two particles separated by a distance  $r$  when both particles are inside the layer. Then, we will consider the number of nearest neighbors (NN) and the distribution of angles between triplets formed by one particle and its two NN. Notice that in order to describe the in-plane structure of a layer the two previous magnitudes should be evaluated for those neighbours standing inside the layer. Moreover, the particles in a layer have additional neighbors in adjacent layers and therefore a more thorough description of the structure will require to account for them in evaluating the total number of NN and the distribution of angles.

### 1. Average ionic density.

The calculation of the mean ionic number density within each slice has revealed that deviations from the bulk value are significant only in the last two slices. At the outermost slice the relative changes in the ionic number density range from  $\approx -11\%$  (Li) to  $9\%$  (Tl) whereas in the previous slice the corresponding values are substantially smaller (see Table III). Note that the average ionic density in the outermost layer decreases in all the alkalis and alkaline-earths, and increases for Tl, Al and Si.

### 2. Transverse pair correlation functions.

In all the systems studied, excepting Tl, the change in  $g_T(r)$  from the bulk to the surface occurs rather abruptly at the outermost layer, because at the second layer its  $g_T(r)$  already coincides with that of the center layer, which in turn is practically identical to the bulk  $g(r)$ . As for Tl, its LV interface is the most structured one, with large oscillations which may indicate an important influence of any given layer on the properties of its surrounding layers. In fact, the change in  $g_T(r)$  from the bulk to the surface is gradual in the case of Tl.

The changes undergone by the average ionic density (Table III) are mirrored by deviations of the associated  $g_T(r)$  with respect to the bulk  $g(r)$ , as evinced by figures 7-9, which show the transverse pair correlation function  $g_T(r)$  at the outer layer. For both alkalis and alkali-earths, the outermost  $g_T(r)$  is displaced towards greater  $r$ -values, in clear correlation with a decreased average ionic density. Conversely, the outermost  $g_T(r)$  for Al, Tl and Si practically preserve the same main peak's position as in the bulk while slightly increasing its height. Notice that in these latter three systems, the ionic number density at the outermost layer did increase with respect to the slab's bulk value.

TABLE IV: Number of neighbors within a layer  $n_{2d}$  for the systems studied.

Metal	$n_{2d}$			
	Layer 1	Layer 2	Layer 3	center layer
Li	4.8	5.3	5.3	5.3
Na	4.5	5.2	5.2	5.2
K	4.6	5.3	5.1	5.1
Rb	4.6	5.1	5.1	5.1
Cs	4.7	5.2	5.2	5.2
Mg	4.9	5.1	5.1	5.1
Ba	4.8	5.3	5.3	5.3
Al	5.1	4.9	4.8	4.8
Tl	5.5	5.5	5.2	5.1
Si	4.1	3.9	4.1	4.0

Conceivably, it might appear that for the alkalis and alkaline-earths those changes in  $g_T(r)$  just amount to an expansion of the system, leading to an increased NN's distance. In the case of Al and Tl the maximum of  $g_T(r)$  does not change position, but the first minimum moves somewhat to the right. The most interesting situation occurs for Si, where apparently some atoms move from the position of a small bump just after the main peak of  $g(r)$  to a distance slightly smaller than the position of the second maximum, yielding a double-second-peak structure in the  $g_T(r)$  of the outermost layer. All these changes induced by the layering of the interface will be thoroughly analyzed in the following section.

### 3. In-plane neighbors.

The number of NN, or coordination number (CN), is usually defined as the average number of neighbors within a distance  $r_{\max}^{2d}$ , identified as the position of either the first minimum of the pair correlation function  $g_T(r)$ , or that of the radial distribution function  $G_T(r)$  (which for these quasi-bidimensional layers is proportional to  $rg_T(r)$  and the average ionic density) of the layer considered. This latter criterion has been used to calculate the results of Table IV although similar trends are found when using the former one. In the alkalis and alkaline-earths there is a competition between the increase of  $r_{\max}^{2d}$  at the outermost layer and the corresponding decrease of the average ionic density. In all cases the latter factor is stronger and we find that the CN,  $n_{2d}$  changes from about 5.2 in the center layer to about 4.7 in the outermost one. In Al and Tl both the average ionic density and  $r_{\max}^{2d}$  increase leading to a somewhat increased CN from the center to the surface. In Si both factors change very little and we find 4 NN (in-plane) both for the center layer and for the outermost one.

Notwithstanding the validity of these results it must be recognized that there is a certain degree of arbitrariness in the definition of when a particle is a “nearest” neighbor

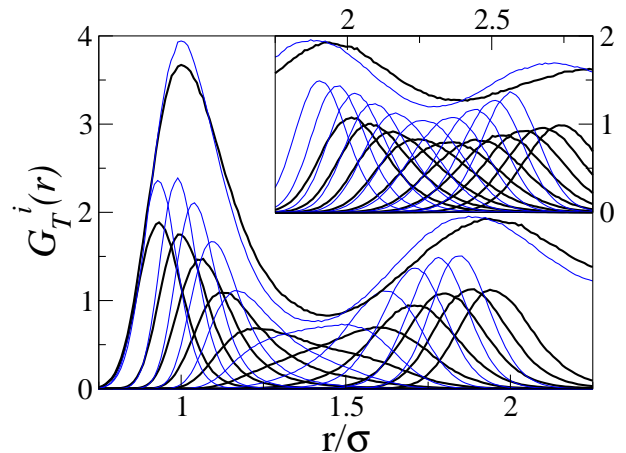


FIG. 10: (Color online) Decomposition of the pair distribution functions for Li in terms of those corresponding to the first, second,  $\dots$ , up to the 20th neighbor. Thick lines: outermost layer, thin blue lines: center layer. Also shown are the associated pair correlation functions,  $g_T(r)$  (scaled so as to fit into the graph).

of another. Some years ago McGreevy and coworkers<sup>29</sup> outlined a proposal for a less arbitrary determination of the CN in computer simulation studies. Their idea is to rewrite the radial distribution function as the sum of the partial functions,  $G_T(r) = \sum_{i=1}^{\infty} G_T^i(r)$ , where  $G_T^i(r)$  is the pair distribution function corresponding to the  $i$ -th neighbor, which indicates the distribution of distances from one particle to its  $i$ -th neighbor. By analyzing the way the different neighbors are distributed, it is possible to discern whether they are inside the first peak, outside it or in between, and therefore it provides a more precise picture of the meaning of the CN. In the present context this idea is even more useful, since by looking at the change of  $G_T^i(r)$  across the LV interface we can better describe the rearrangement of the particles induced by the layering of the interface.

In figures 10-12 we show this decomposition of  $G_T(r)$  for Li (which stands as a representative example of the alkalis and alkaline-earths, because all of them show the same behavior), Al and Si. Note that in all cases the amplitudes of  $G_T^i(r)$  follow closely the shape of the pair correlation function,  $g_T(r)$ , of the layer considered.

Let us consider first the case of Li at the center layer. It is found that the neighbors up to the fourth are well below the first peak of  $g_T(r)$ , and the fifth neighbor, despite being more spread out, can reasonably be assigned to the set of “nearest” neighbors. The sixth one, however, is clearly distributed between the first and second peaks of  $g_T(r)$ . The second peak is spawned by part of the sixth neighbor, the neighbors number 7 to 15 and again partly the 16th one. From this analysis one could assign 5.4 and 10.1 neighbors to the first and second coordination shells respectively. In the case of the outermost layer we find 4 neighbors well inside the first peak of  $g_T(r)$ , whereas the



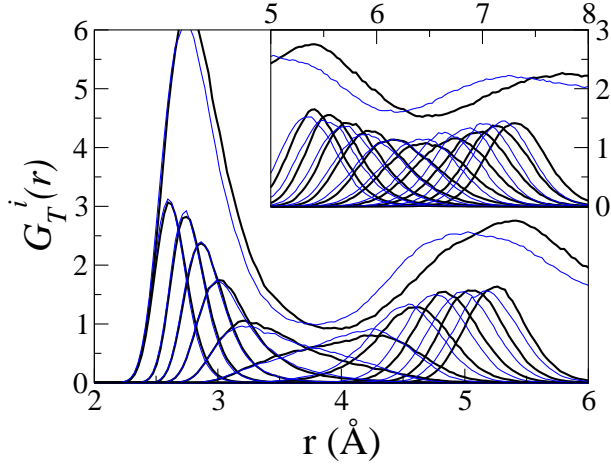


FIG. 11: (Color online) Same as the previous figure but for Al.

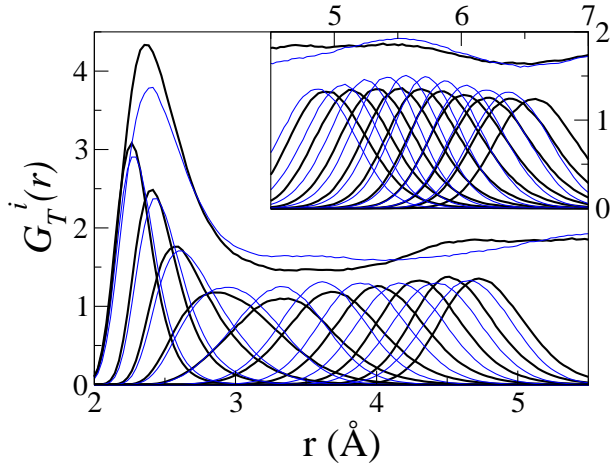


FIG. 12: (Color online) Same as the previous figure but for Si.

fifth and sixth neighbors are very spread out, both being shared by the first and second peaks of  $g_T(r)$ . The rest of the second peak is due to neighbors number 7 to 15 and part of the 16th one. We can therefore ascribe values of 5 and 10.5 to the first and second CNs. In order to separate out the effects of the decrease of the average ionic density, the comparison between the  $G_T^i(r)$  of the center layer and that of the outermost one is made for Li by rescaling the distances by  $\sigma$ , which denotes the position of the maximum of  $g_T(r)$ . In this way we observe that the expansion is not uniform: the peak positions of  $G_T^1(r)$  to  $G_T^3(r)$  remain unchanged (in units of  $\sigma$ ) but from the 4th neighbor onwards there is more than uniform expansion and already the 6th neighbor in the outermost layer is located at the position of the 7th one in the bulk, while the 12th neighbor in the outermost layer is located at the position of the 14th one in the center.

For liquid Al the rearrangement of atoms at the inter-

face is very small. The first five neighbors hardly change, whereas starting at the sixth neighbor a small expansion occurs, followed again by contraction so that the positions of the 15th neighbors again coincide. Analyzing the distribution of atoms under the first and second peaks, the CNs for the first and second shell would be 5.0 and 9.5 in the center and 5.2 and 10.3 at the surface.

In Si we find that the small bump after the main peak of the bulk  $g(r)$  is due to the particular distribution of the fifth and sixth neighbors, the first four being clearly located under the main peak, which leads to a CN of 4.0 atoms, both in the center and at the surface. When one comes to the outermost layer the heights of  $G_T^5(r)$  and  $G_T^6(r)$  are depleted, whereas the following neighbors up to the 16th attain very similar distributions although of course at increasing distances, yielding this way the double-peak structure of the second peak of  $g_T(r)$ . Therefore the previous interpretation of some atoms moving from the bump to the second peak is not correct; the position of the fifth neighbor is exactly the same in the surface and in the bulk, and starting from the sixth neighbor a weak expansion does occur, but it amounts to one atom only at large distances: the 18th surface neighbor is located at the position of the 19th bulk neighbor.

#### 4. In-plane bond-angle distribution functions.

The usual way to calculate the bond-angle distribution function is to choose an atom and compute the angle between the lines joining this atom and two of its NN, which would mean that they are separated less than  $r_{max}^{2d}$  from the first one. However, following the ideas of the previous section we compute the angle between the lines joining the central atom and any two atoms taken from its first  $i$  neighbors. It is interesting to analyze the evolution of the bond-angle distributions,  $P_i(\theta)$ , as more NN are included by starting at  $i = 2$  and up to the integer closest to the CN. Figure 13 shows the obtained results for liquid Li and Si.

Starting with Li, we observe that in the center layer the distribution of cosines of angles peaks near 0.5,  $-0.5$  and  $-1$  (angles 60, 120 and 180 degrees) suggesting that the local environment is mainly hexagonal, even though the CN is around 5 (in a pentagonal environment the peaks would occur at 0.309 and  $-0.809$  very far from the observed ones). As we increase the number of neighbors included in the calculation the peak around 60 degrees moves towards smaller angles, whereas the one near 120 degrees becomes fuzzier while hardly changing its position. The picture in the outermost layer is rather similar though the peak near 120 degrees is reduced to a shoulder in favor of an enhanced peak at 180 degrees.

The case of Si, with a more open structure, shows a much stronger variation in the bond-angle distributions as more neighbors are included in the calculation. Starting with the center layer, we observe a clear peak near

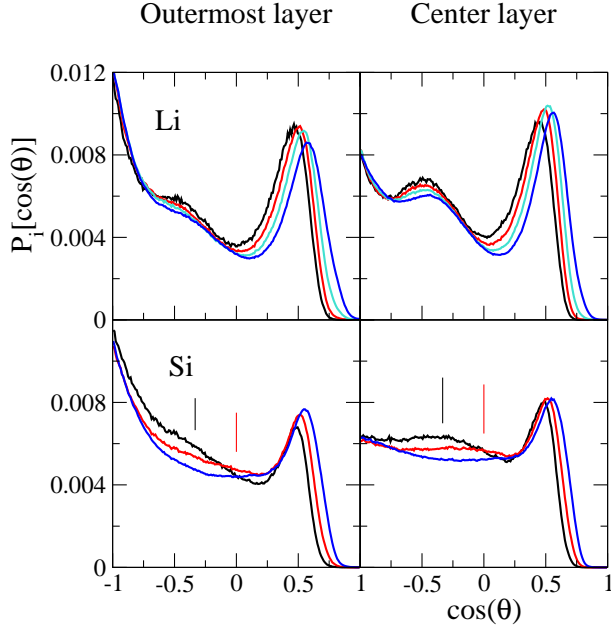


FIG. 13: (Color online) Bond-angle distribution functions for Li and Si at different layers of the interface. The number of neighbors included in the calculation increases from 2 towards the coordination number (5 for Li, 4 for Si) as the position of the peak near  $\cos \theta = 0.5$  moves to the right. The vertical lines indicate the cosines of the tetrahedral angle (109.5 degrees) and of 90 degrees.

60 degrees, which moves towards smaller angles if more neighbors are included. However, if only the first two neighbors are included a faint feature also appears near the tetrahedral angle, when including up to the third neighbor, this feature moves to an angle near 90 degrees, and if we consider all the neighbors up to the fourth, the feature completely disappears. The variations brought about at the surface layer are similar as those observed in Li: we find an enhanced peak at 180 degrees, while the small features observed at the center layer for intermediate angles show up as shoulders, which also move their position from tetrahedral to 90 degrees and to disappearance when including 2, 3 or 4 neighbors in the computation.

##### 5. Total number of neighbors.

To analyze the local 3-dimensional structure of the atoms at the different layers, we have computed the corresponding  $z$ -dependent CN,  $n(z)$ , by counting the average number of neighbors (whatever be their position) within a distance  $r_{\max}^{3d}$  taken as the position of the first minimum of the bulk pair distribution function (proportional to  $r^2 g(r)$ ). Our results, which are summarized in Table V, show that for most of the slab  $n(z)$  remains invariable and close to that of the bulk system and only very

TABLE V: Values of the  $z$ -dependent coordination number,  $n(z)$  at different  $z$ -values along the slab.  $n(z_B)$  is the average value in a wide region around the center of the slab.  $z_{OM}$  and  $z_{SM}$  are the positions (in Å) of the outermost and second maximum respectively.  $z_d$  is the distance (in Å) between the outermost maximum and the inflection point at the decaying ionic density profile, and  $n(z_d)$  is defined in the text.

Metal	$n(z_B)$	$z_{OM}$	$n(z_{OM})$	$z_{SM}$	$n(z_{SM})$	$z_d$	$n(z_d)$
Li	11.85	24.7	7.9	22.4	11.3	1.05	7.8
Na	11.60	31.1	7.9	28.3	11.2	1.30	7.6
K	11.90	30.9	7.9	27.4	11.5	1.45	7.8
Rb	12.00	34.5	8.1	30.9	11.7	1.55	7.8
Cs	12.00	39.9	8.0	35.8	11.5	1.80	7.8
Mg	11.50	26.4	7.9	23.9	11.3	1.25	7.7
Ba	12.00	31.8	8.1	28.4	11.6	1.60	7.9
Al	11.30	18.7	7.9	16.35	11.2	1.05	7.6
Tl	11.90	27.5	8.2	24.6	11.9	1.0	7.6
Si	5.9	18.8	4.5	16.3	5.8	1.15	4.3

close to the interface, namely starting around the second outer maximum,  $n(z)$  begins to decrease. Aside from liquid Si, all the other systems have an average bulk CN,  $n(z_B) \approx 12$ , which is reduced by  $\approx 1/3$  at their respective outer maximum, namely  $n(z_{OM}) \approx 8$ . Liquid Si has a noticeably smaller  $n(z_B) \approx 6$ , decreasing to  $\approx 4.5$  at the surface, because of some remnants of covalent bonding in the liquid, which induce an open structure with an experimental value of around 5.7<sup>31</sup>- 6.4<sup>32</sup> neighbours. For comparison, we note that the KS-AIMD calculations of Fabricius *et al*<sup>11</sup> for liquid Si yielded  $n(z_B) \approx 6.4$  which reduced to 5.3 at the outermost maximum. Indeed, this decrease in CN is a well known feature at surfaces, produced by the lack of atoms outside the interface. In the next section we will discuss if (and how) the remaining neighbors redistribute in this outer part of the system.

As for the structural rearrangements induced by the interface, Fabricius *et al*<sup>11</sup> have proposed to quantify those changes by comparison with an ideally terminated surface obtained by cutting abruptly the slab in the central region, i.e. at  $z = 0$ . Then, we evaluate  $n(z)$  at a distance  $z_d$  which is approximately the distance between the outermost maximum and the inflection point in the respective ionic DP. The obtained values are shown in Table V and they are slightly smaller than those at the outer maximum which suggests that the surface structural rearrangement induces some minor increase of the CN of an ideally terminated surface.

##### 6. Total bond-angle distribution functions.

Again, instead of the usual way of defining a NN as one separated by at most  $r_{\max}^{3d}$  from the central one, we compute the bond angles between a particle and two of its first  $i$  neighbors, with emphasis on  $i$  being either 2 or the integer value closest to the (3-dimensional) CN. Figure

14 depicts the results obtained for the bond-angle distribution functions in Li and Si. Specifically, we show the results obtained by counting only the first two neighbors in the calculation as well as those obtained by considering the corresponding CN, which amounts to 8 neighbors for Li at the outermost layer and 12 at the inner ones, and 4 neighbors for Si at the surface, and 6 at the second and center layers.

In both systems we find that when the calculation includes all the NN (the full CN), then the bond-angle distribution at the surface closely resembles that at the inner layers, including the bulk; however, we stress that this result relies on taking the CN associated to each layer, otherwise the distributions would peak at somewhat different angles. The more probable angles are somewhat smaller than those reflecting a perfect icosahedral environment in Li, and around 60 degrees and a somewhat smaller angle than the tetrahedral one in Si.

On the other hand, if the calculation includes only the first two neighbors, then the obtained bond-angle distribution describes a situation where the disorder induced by the distance is somehow at its minimum level, thus reflecting the “most local” bond distribution. The results shown on the left panels of figure 14 provide evidence that in the case of Si, the surface has practically no influence on the bond-angle distribution which now shows a peak around 60 degrees and another one at exactly the tetrahedral angle. For liquid Li we find peaks close to the icosahedral angles in the inner layers, but at the surface we observe a redistribution of bonds with an increased number of bonds at around 60 degrees along with an important depletion at larger angles. However, the peak’s positions do not change appreciably and remain around the icosahedral angles.

### C. Electronic structure.

Figures 1-5 show the calculated self-consistent valence electronic DP which also exhibit some oscillations although with much smaller amplitudes than those of the associated longitudinal ionic DP. However, the most remarkable feature refers to the relative phases between the longitudinal ionic and valence electronic DP. According to Figures 1-5 all situations are allowed with the relative phase evolving from an opposite one, as it happens for all the alkalis, to being almost in-phase for Si.

This is an unexpected feature because the scant previous studies on the longitudinal ionic and the valence electronic DP<sup>9,33</sup> had always yielded an opposite phase. Specifically, the Monte Carlo calculations of Rice and coworkers<sup>9</sup> for the LV interface in liquid Na, Cs and Ga produced longitudinal ionic and valence electronic DP standing in nearly perfect opposite phase. This feature was rationalized in terms of a competition between the valence electronic kinetic energy contribution, which gets smaller values by damping the oscillations, and the interaction term between electrons and ions, (mainly its

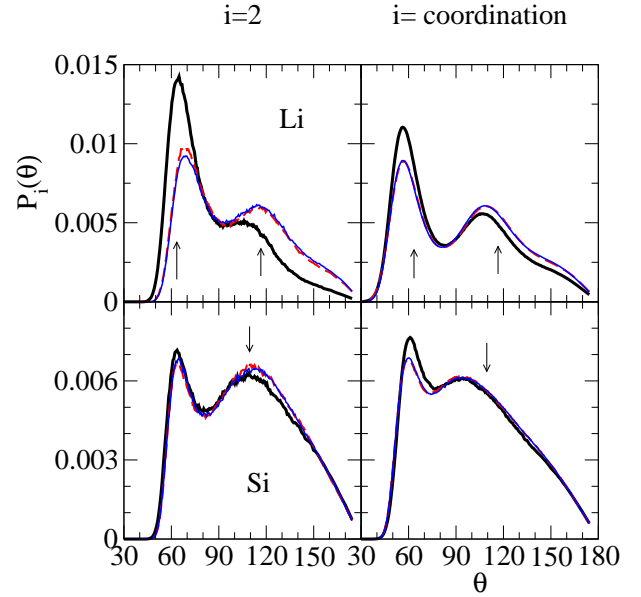


FIG. 14: (Color online) Total bond-angle distribution functions for Li and Si. Thick line: outermost layer. Dashed red line: second layer. Thin blue line: center layer. The number of neighbors included in the calculation is 2 for the left panels and the coordination number for the right panels. The arrows indicate the icosahedral angles (63.4 and 116.6 degrees) for Li and the tetrahedral angle (109.4 degrees) for Si.

coulombic part), which being attractive takes smaller values for in-phase oscillations. Furthermore, the OF-AIMD simulations by Jesson and Madden<sup>33</sup> for the structure of the liquid-solid interface in Al also gave a longitudinal valence electronic DP standing in a opposite phase with the ionic one in both the crystalline and liquid phases. This behaviour was now explained in terms of the interaction, embodied in the pseudopotential, between valence and core electrons, which tends to exclude the valence electrons from the ionic positions.

In fact, the assumption of an opposite phase between the longitudinal ionic and valence electronic DP has been widely assumed; however a closer scrutiny, based on the present calculations, reveals some weak points on the previous explanations. First, our results for the valence electronic kinetic energy show that it takes very small values (less than 5% for all systems in this work) in comparison with those of the valence electron-ion interaction term; therefore the idea of assigning to the valence electronic kinetic energy any relevant role in establishing the phase of the valence electronic DP oscillations appears baseless. Second, all the systems considered in this work, have *s*-type valence electrons which in some cases (Al, Tl and Si) are also joined by *p*-type electrons. Taking into account that the *s*-type valence electronic density attains a maximum value at the ionic positions, it now appears rather surprising to find systems, specially those with *s*-type valence electrons only, in which both profiles

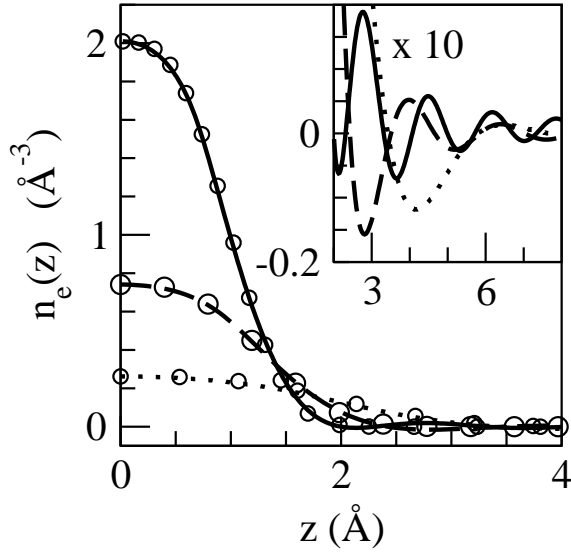


FIG. 15: Valence pseudoatomic densities for K (dotted line), Mg (dashed line) and Si (full line); the inset depicts its shape (multiplied by a factor of ten) for larger distances. The open circles represent the analytical model proposed in the text.

were not in-phase. Consequently, we have undertaken several tests in order to ascertain the mechanisms underlying the phase-shift between the longitudinal ionic and valence electronic DP.

First, we have constructed a valence electronic DP in the slab by performing a linear superposition of the valence pseudoatomic density calculated within the process of constructing the local ionic pseudopotential. We recall that the valence pseudoatomic density, which was obtained by means of a KS-type calculation, is a spherically symmetric function and in order to analyze its role in setting the shape of the valence electronic DP, we have first integrated over its  $x$  and  $y$ -dependencies; the resulting function  $n_e(z)$ , which is the one effectively used in the calculation of the valence electronic DP in the slab, is plotted for some representative systems, in figure 15. For all systems, the corresponding  $n_e(z)$  shows a decaying behavior whose width along with the associated weak Friedel oscillations may be identified as its basic characteristic features. The calculation of the valence electronic DP in the slab has proceeded as follows: by taking the OF-AIMD generated ionic positions we have located at each ionic position the previous  $n_e(z)$  and we have carried out a configurational average. This approach is consistent with a linear response treatment of the valence electron density and therefore lacks any competition between kinetic and coulombic effects. The resulting valence electronic density profiles are compared with the OF-AIMD self-consistent ones for K, Mg and Si in figure 16, which shows that both profiles are remarkably similar to each other. In particular, the phase of the valence electronic density oscillations is preserved, which suggests that the phase-shift must be determined by some feature embod-

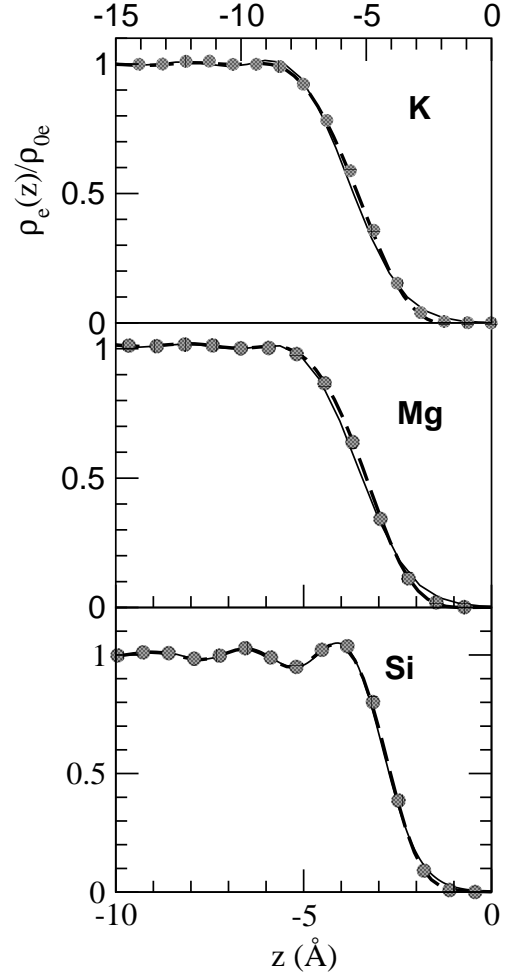


FIG. 16: Valence electronic density profiles (relative to the bulk average value) for the K, Mg and Si liquid-vapour interfaces. The continuous line is the OF-AIMD result, the dashed line represents a linear superposition of displaced densities and the grey circles are a linear superposition of the model densities, without Friedel oscillations.

ied in the valence pseudoatomic density.

In order to analyze the different roles played by both features in modulating the phase-shift between the longitudinal ionic and valence electronic DP, we have fitted the  $n_e(z)$  to a model that shows no Friedel oscillations but otherwise accurately reproduces its shape. We found that a rather good fit can be obtained for a model density of the normalized form  $\exp[-|z/\sigma|^3]$ , which includes just one parameter,  $\sigma$ . The specific values for the all the different systems are given in Table II which shows a range of variation from  $\sigma = 2.71$  Å in Cs to  $\sigma = 1.132$  Å for Si. Furthermore, a comparison between the  $n_e(z)$  and the above fitting model, is depicted in Figure 15 for K, Mg and Si. Besides the absence of the Friedel oscillations, it is observed that the model provides a rather good description of  $n_e(z)$  for all the systems in this work. Now, by using the fitted model densities we have again

performed its superposition according to the OF-AIMD generated ionic positions and the obtained valence electron profiles are shown in figure 16 for K, Mg and Si. Once again we observe that the corresponding valence electronic DP is virtually indistinguishable, for all systems, from that obtained by the superposition of valence pseudoatomic densities. More interestingly, the phase of the oscillations is preserved, and this fact suggests that the Friedel oscillations of the valence pseudodensity are irrelevant for this question. Therefore, the reason for the different phase-shifts between ionic and valence electron oscillations must be found in the width of the valence pseudoatomic density (quantified by the parameter  $\sigma$ ) as compared to the distance between layers in the profile (quantified by the wavelength of the longitudinal ionic oscillations  $\lambda$ ). The ratio  $\sigma/\lambda$  takes the values 0.62, 0.58 and 0.45 for K, Mg and Si respectively, which moreover correlates with a decreasing phase difference between their associated longitudinal ionic and valence electronic DPs. Table II lists the obtained values of  $\sigma/\lambda$  for all the systems considered in this work and three groups can be discerned: (i) the alkalis where  $0.62 \leq \sigma/\lambda \leq 0.64$ , (ii) Mg, Ba and Al with  $0.55 \leq \sigma/\lambda \leq 0.59$ , and (iii) Tl and Si where  $0.44 \leq \sigma/\lambda \leq 0.47$ . Within each group, there is a similar phase difference between the corresponding longitudinal ionic and valence electronic DPs as epitomized by K, Mg and Si which may be considered as representatives for each group.

As a further check on the previous argument, we have performed another test for the K, Mg and Si slabs. By taking their respective OF-AIMD generated ionic positions, we have again carried out a superposition of model densities with different widths, namely  $\sigma/\lambda \approx 0.45$ , 0.575 and 0.625, which may be considered as representative values of the previous three groups. The calculated valence electronic DPs are depicted in figure 17 which shows that, in the three systems, the resulting valence electronic DPs move from being nearly in-phase (when  $\sigma/\lambda \approx 0.45$ ) towards nearly opposite phase (when  $\sigma/\lambda \approx 0.625$ ) with respect to the corresponding longitudinal ionic DP. These results clearly showcase the crucial role played by the ratio  $\sigma/\lambda$  in establishing the phase-shifts between the longitudinal ionic and valence electronic DPs. Moreover, the previous results provide a rationale for the aforementioned phase-shifts between the ionic and valence electronic DPs obtained for liquid Al in the present calculations and the OF-AIMD simulations of Jesson and Madden<sup>33</sup>. Specifically, our OF-AIMD results for the liquid-vapor interface of Al yielded  $\lambda = 2.35$  Å, (with a ratio  $\sigma/\lambda \approx 0.548$ ), whereas those of Jesson and Madden, which referred to liquid Al in contact with the (100) face of its solid fcc phase, gave  $\lambda \approx 2.1$  Å (which is close to the interlayer distance in the solid) and therefore leads to a  $\sigma/\lambda \approx 0.613$ . This latter ratio is close to the range obtained for the alkalis and therefore it foretells an opposite phase between the longitudinal ionic and valence electronic DPs, in accordance with Jesson and Madden's results.<sup>33</sup>

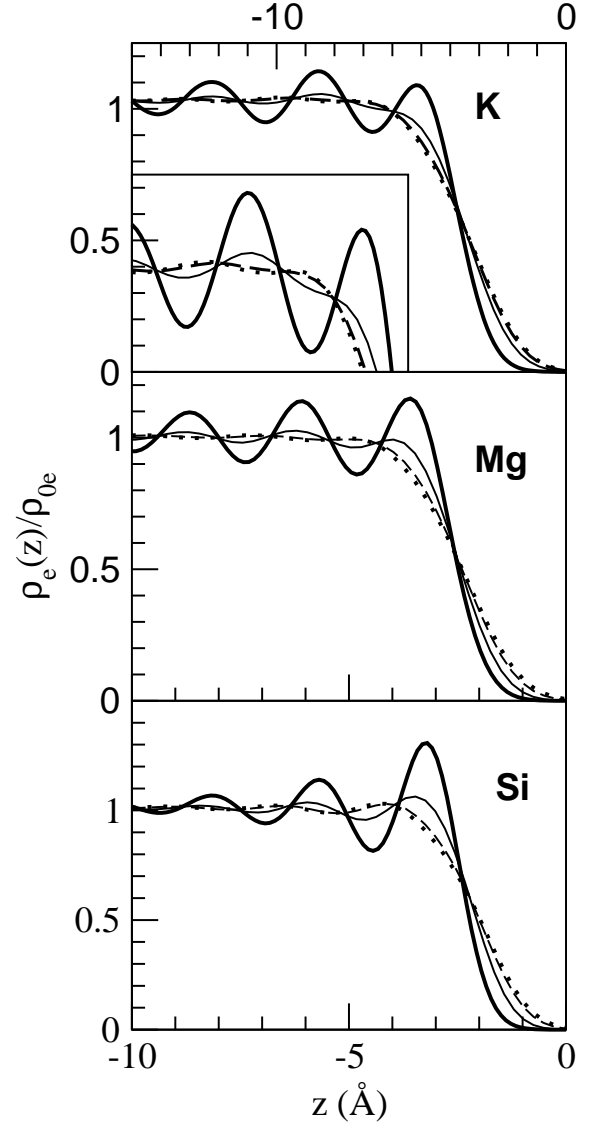


FIG. 17: Valence electronic density profiles obtained by superposition of model densities with different  $\sigma/\lambda$  values, namely  $\sigma/\lambda = 0.45$  (full line), 0.575 (broken line) and 0.625 (dotted line). The thick line represents the longitudinal ionic density profile and the inset for K depicts the two outermost maxima.

Experimental study of the LV interface is usually performed by X-ray reflectivity and/or grazing incidence X-ray diffraction techniques. Both methods measure the total electronic density profile which is the sum of both the core and valence electronic density contributions. Whereas the valence electronic DP is obtained by the OF-AIMD method, the corresponding core electronic DP has been calculated as follows. Using the OF-AIMD generated ionic positions we have placed at each ionic position the core electronic density (already computed in the process of calculating of the local pseudopotential) and we have carried out a configurational average. Once again,

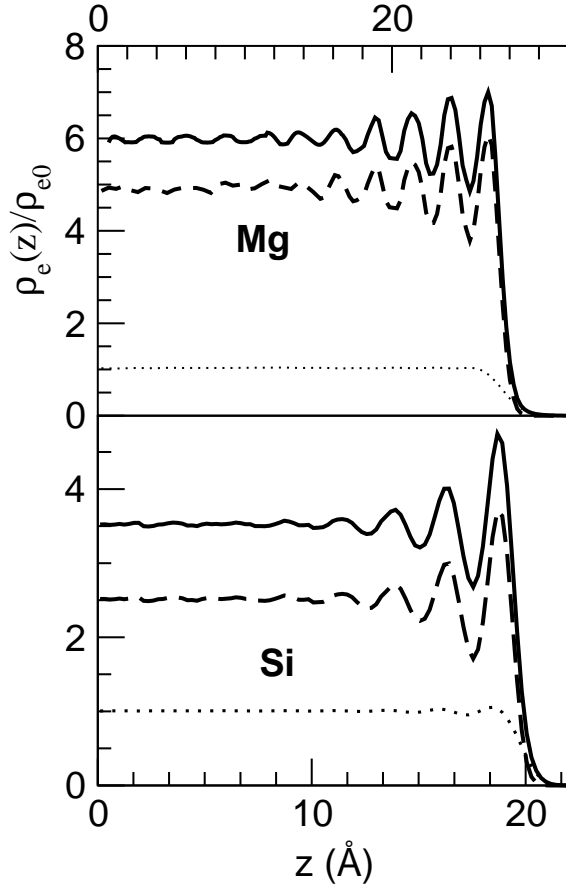


FIG. 18: Valence (dotted line), core (dashed line) and total (full line) electronic density profiles (relative to the valence bulk value) for liquid Mg and Si. The longitudinal ionic DP is indistinguishable from the total electronic one.

we note that the core electronic density is a spherically symmetric function which has previously been integrated over its  $x$  and  $y$ -dependencies yielding a function  $n_c(z)$ , which is the one effectively used in the calculation of the core electronic DP. Figure 18 shows, for the Mg and Si slabs, a comparison among the obtained valence, core and total electronic DPs. Since the core electronic densities  $n_c(z)$ , are rather narrow functions, their superposition leads to a core electronic DP which stands clearly in phase with the longitudinal ionic DP. Consequently, when it is added to the valence electronic DP it yields a total electronic DP whose phase-shift with respect to the longitudinal ionic DP depends on both the relative weight of the core electronic DP (always in phase) and the valence electronic DP (any phase is possible) as well as on the amplitude of the oscillations in both DPs. For the particular cases of Mg and Si, which are plotted in Figure 18, their valence electronic DPs have relative weights of  $1/6$  and  $2/7$  respectively and, moreover, the oscillations in their core electronic DPs are of substantially larger amplitude than those in their respective valence electronic DPs. Both features cooperate so as to produce a total

electronic DP which practically coincides with longitudinal ionic DP. Indeed, this is a common trait in all the metallic systems considered in this work. Even liquid Li, which *a priori* could be more prone to changes because its valence electronic DP has a relative weight of  $1/3$  and also stands in opposite phase with the core electronic DP, has a total electronic DP which closely matches the ionic one.

#### IV. CONCLUSIONS

Results have been reported for the structure of the LV interface in several simple *sp*-bonded liquid metals. They have been obtained by an *ab initio* molecular dynamics method based on the density functional theory. Although it employs an approximate electronic kinetic energy functional, the large variations in electron density associated with the liquid-vapour interface are accounted for selfconsistently in the forces acting among the ions. The MD simulations were performed by using simulation slabs composed of 2000 ions, which are wide enough to discard possible interference effects between the two free surfaces.

The calculated longitudinal ionic and electronic DPs exhibit clear oscillations, with the ionic ones lasting for at least four layers into the bulk liquid. The wavelength of the ionic oscillations shows good scaling with the radii of the associated Wigner-Seitz spheres; conversely no definite relationship with electronic parameters has been found. Furthermore, the metals with the greater valence display ionic DPs with the higher amplitude of the outer oscillation as well as a steeper decaying tail in the LV interface region.

Several structural properties were calculated, with special attention devoted towards its evolution along the outermost layers. Results were presented for the transverse pair distribution functions which in turn are used to analyze the atomic rearrangements occurring at LV interface. The coordination numbers remain practically constant for most of the slab and only very close to the LV interface there is a reduction related to the absence of neighbors outside the interface. However, when compared properly, we have found that the angular distribution of the nearest neighbors doesn't change significantly across the interface. Moreover, it is shown that the interface induces weak structural rearrangements as compared with an ideally, step-like, terminated surface.

The valence electronic DPs show oscillations near the LV interface which are much weaker than those of the associated ionic DP. Moreover, it was found that the valence electronic DP is practically reproduced by superposing, at the ionic sites, the pseudoatomic valence densities calculated in the process of constructing the local pseudopotential. This suggests that for each system, the main features of its self-consistent valence electronic DP are already embodied in the characteristics of the corresponding pseudoatom valence density.



We have also analyzed the mechanisms behind the relative phases of the oscillations in the ionic and valence electronic DPs. It is found that those phases evolve from opposite phase in the alkalis to almost in-phase for Si. This is in stark contrast with the accepted wisdom, namely that the electronic and ionic DPs should oscillate in opposite phase. An explanation is provided in terms of the size of the pseudoatoms (ion plus valence electronic cloud) relative to the distance between consecutive layers of the ionic profile.

## Acknowledgments

DJG and LEG acknowledge the financial support of the DGICYT of Spain (MAT2005-03415) and the EU FEDER program. MJS acknowledges the support of the NSERC of Canada.

- 
- <sup>1</sup> J.S Rowlinson and B. Widom in *Molecular Theory of Capillarity* (Clarendon, Oxford 1982); D. Beaglehole in *Fluid Interfacial Phenomena* edited by C. A. Croxton (Wiley, New York 1986)
  - <sup>2</sup> J. Penfold, Rep. Prog. in Phys. **64**, 777 (2001)
  - <sup>3</sup> B. Groh, R. Evans and S. Dietrich, Phys. Rev. E, **57**, 6944 (1998); M. Gonzalez-Melchor, J. Alejandro and F. Bresme, Phys. Rev. Letters **90**, 135506 (2003)
  - <sup>4</sup> D. Beaglehole, Phys. Rev. Letters **43**, 2016 (1979); Physica B **100**, 163 (1980)
  - <sup>5</sup> B. M. Ocko, A. Braslau, P.S. Pershan, J. Als-Nielsen and M. Deutsch, Phys. Rev. Letters **57**, 94 (1986); Y. Martinez-Raton, A. Somoza, L. Mederos and D. Sullivan, Faraday Discuss. **104**, 111 (1996)
  - <sup>6</sup> R. Evans, *Fundamentals of Inhomogeneous Fluids*, edited by D. Henderson (Dekker, New York 1992)
  - <sup>7</sup> S. W. Barton, B.N. Thomas, F. Novak, P.M. Weber, J. Harris, P. Dolmer, J.M. Bloch and S.A. Rice, Nature (London) **321**, 685 (1986)
  - <sup>8</sup> M. P. D'Evelyn and S. A. Rice, Phys. Rev. Letters **47**, 1844 (1981); M. P. D'Evelyn and S. A. Rice, J. Chem. Phys. **78**, 5225 (1983); J.G. Harris, J. Gryko and S.A. Rice, J. Chem. Phys. **87**, 3069 (1987)
  - <sup>9</sup> M. Zhao, D. S. Chekmarev, Z. H. Cai and S. A. Rice, Phys. Rev. E **56**, 7033 (1997); D. Chekmarev, M. Zhao and S. A. Rice, J. Chem. Phys. **109**, 768 (1998); D. S. Chekmarev, M. Zhao and S. A. Rice, Phys. Rev. E **59**, 479 (1999)
  - <sup>10</sup> D. Chekmarev, M. Zhao and S. A. Rice, J. Chem. Phys. **109**, 1959 (1998)
  - <sup>11</sup> G. Fabricius, E. Artacho, D. Sanchez-Portal, P. Ordejon, D.A. Drabold and J.M. Soler, Phys. Rev. B **60**, R16283 (1999)
  - <sup>12</sup> B.G. Walker, C. Molteni and N. Marzari, J. Phys: Condens. Matter **16**, S2575 (2004)
  - <sup>13</sup> D.J. González, L.E. González and M.J. Stott, Phys. Rev. Letters **92**, 085501 (2004); Phys. Rev. Letters **94**, 077801 (2005); J. Chem. Phys. **123**, 201101 (2005)
  - <sup>14</sup> M. A. Gómez and E. Chacón, Phys. Rev. B **46**, 723 (1992); Phys. Rev. B **49**, 11405 (1994)
  - <sup>15</sup> O. M. Magnussen, B. M. Ocko, M.J. Regan, K. Penanen, P.S. Pershan and M. Deutsch, Phys. Rev. Lett. **74**, 4444 (1995); M. J. Regan, E.H. Kawamoto, S. Lee, P.S. Pershan, N. Maskil, M. Deutsch, O.M. Magnussen, B. M. Ocko and L.E.Berman, Phys. Rev. Lett. **75**, 2498 (1995); E. DiMasi, H. Tostmann, B. M. Ocko, P.S. Pershan and M. Deutsch, Phys. Rev. B **58**, R13419 (1998); H. Tostmann, E. DiMasi, P. S. Pershan, B. M. Ocko, O. G. Shpyrko and M. Deutsch, Phys. Rev. B **59**, 783 (1999); H. Tostmann, E. DiMasi, P.S. Pershan, B. M. Ocko, O.G. Shpyrko and M. Deutsch, Phys. Rev. B **61**, 7284 (2000); O. Shpyrko, P. Huber, A. Grigoriev, P. Pershan, B. Ocko, H. Tostmann and M. Deutsch, Phys. Rev. B **67**, 115405 (2003); O.G. Shpyrko, A.Y. Grigoriev, C. Steimer, P.S. Pershan, B. Lin, M. Meron, T. Graber, J. Gerbhardt, B. Ocko and M. Deutsch, Phys. Rev. B **70**, 224206 (2004)
  - <sup>16</sup> S. Iarlori, P. Carnevali, F. Ercolessi and E. Tosatti, Surf. Sci. **211/212**, 55 (1989);
  - <sup>17</sup> E. Chacón, M. Reinaldo-Falagan, E. Velasco and P. Tarazona, Phys. Rev. Letters **87**, 166101 (2001); E. Velasco, P. Tarazona, M. Reinaldo-Falagan and E. Chacón, J. Chem. Phys. **117**, 10777 (2002)
  - <sup>18</sup> P. Hohenberg and W. Kohn, Phys. Rev. **136**, 864 (1964); W. Kohn and L.J. Sham, Phys. Rev. **140**, A1133 (1965)
  - <sup>19</sup> D. J. González, L. E. González, J. M. López and M. J. Stott, Phys. Rev. B **65** 184201 (2002); J. Phys.: Cond. Matter **13** 7801 (2001)
  - <sup>20</sup> F. Perrot, J. Phys: Condens. Matter **6**, 431 (1994); E. Smargiassi and P. A. Madden, Phys. Rev. B **49**, 5220 (1994); M. Foley and P. A. Madden, Phys. Rev. B **53**, 10589 (1996)
  - <sup>21</sup> M. Schmidt, R. Kusche, W. KronMüller, B. von Issendorff and H. Haberland, Phys. Rev. Lett. **79**, 99 (1997); M. Schmidt, R. Kusche, B. von Issendorff and H. Haberland, Nature (London) **393**, 328 (1998); R. Kusche, T. Hippler, M. Schmidt, B. von Issendorff and H. Haberland, Eur. Phys. J. D **9**, 1 (1999); M. Schmidt and H. Haberland, Comptes Rendus Physique **3**, 327 (2002); M. Schmidt, J. Donges, Th. Hippler and H. Haberland, Phys. Rev. Lett. **90**, 103401 (2003)
  - <sup>22</sup> A. Aguado and J. M. López, Phys. Rev. Lett. **94**, 233401 (2005); A. Aguado, J. Phys. Chem. B **109**, 13043 (2005)
  - <sup>23</sup> L. E. González and D. J. González, arXiv:cond-mat/0606130
  - <sup>24</sup> H. Göbel and P. von Blanckenhagen, Phys. Rev. B **47**, 2378 (1993)
  - <sup>25</sup> Ismail, E. W. Plummer, K. Lazzeri and S. de Gironcoli, Phys. Rev. B **63**, 233401 (2001)
  - <sup>26</sup> N. Marzari, D. Vanderbilt, A. de Vita and M. C. Payne, Phys. Rev. Lett. **82**, 3296 (1999)
  - <sup>27</sup> A. Delisle, D. J. González and M. J. Stott, Phys. Rev. B **73**, 064202 (2006)
  - <sup>28</sup> J. Blanco, D. J. González, L. E. González, J. M. López and M. J. Stott, Phys. Rev. E **67** 041204 (2003); D. J. González, L. E. González, J. M. López and M. J. Stott, Phys. Rev. E **69** 031205 (2004)
  - <sup>29</sup> R. L. McGreevy, A. Baranyai and I Ruff, Phys. Chem.

- Liquids **16**, 47 (1986)
- <sup>30</sup> Y. Waseda, in *The Structure of Non-Crystalline Materials* (McGraw-Hill, New York 1980)
- <sup>31</sup> S. Takeda, Jpn. J. Appl. Phys. **34**, 4889 (1995)
- <sup>32</sup> Y. Waseda and K. Suzuki, Z.Phys. B **20**, 339 (1975)
- <sup>33</sup> B.J. Jesson and P.A. Madden, J. Chem. Phys. **113**, 5935 (2000)